

Modulation of Monsoon Circulations by Cross-Equatorial Ocean Heat Transport

Nicholas J. Lutsko*

3 Nicholas J. Lutsko*

Department of Earth, Atmospheric, and Planetary Sciences, Massachusetts Institute of Technology, Cambridge, Massachusetts

John Marshall

Department of Earth, Atmospheric, and Planetary Sciences, Massachusetts Institute of Technology, Cambridge, Massachusetts

Brian Green

*Joint Institute for the Study of the Atmosphere and Ocean, University of Washington, Seattle,
Washington*

¹² *Corresponding author address: Nicholas Lutsko, Department of Earth, Atmospheric, and Planetary Sciences, Massachusetts Institute of Technology, Cambridge, Massachusetts
¹³

¹⁴ E-mail: lutsko@mit.edu

ABSTRACT

Motivated by observations of southwards ocean heat transport (OHT) in the Northern Indian Ocean during summer, the role of the ocean in modulating monsoon circulations is explored by coupling an atmospheric model to a slab ocean with an interactive representation of OHT and an idealized subtropical continent. Southwards OHT by the cross-equatorial cells is caused by Ekman flow driven by southwesterly monsoon winds in the summer months, cooling sea-surface temperatures (SSTs) south of the continent. This increases the reversed meridional surface gradient of moist static energy, shifting the precipitation maximum over the land and strengthening the monsoonal circulation, in the sense of enhancing the vertical wind shear. However, the atmosphere's cross-equatorial meridional overturning circulation is also weakened in the presence of southwards OHT, as the atmosphere is required to transport less energy across the equator. The sensitivity of these effects to varying the strength of the OHT, fixing the OHT at its annual-mean value and to removing the land are explored. Comparisons with more realistic models suggest that the idealized model used in this study produces a reasonable representation of the effect of OHT on SSTs south of subtropical continents, and hence that OHT plays an important role in shaping monsoon circulations on Earth.

³³ **1. Introduction**

³⁴ It is now well understood that the South Asian monsoon is a thermally-direct circulation driven
³⁵ by the thermodynamic contrast which develops in the summer months between the Indian subcon-
³⁶ tinent and the Indian Ocean to the south (e.g., Plumb and Hou (1992); Privé and Plumb (2007a);
³⁷ Privé and Plumb (2007b); Bordoni and Schneider (2008); Zhai and Boos (2015); Geen et al.
³⁸ (2018)). Intuitively, this contrast arises because the land's smaller heat capacity causes it to warm
³⁹ up faster in the summer than the surrounding waters, but recent work has shown that a number of
⁴⁰ other factors are required to maintain the gradient. Most importantly, the Himalayas play a crucial
⁴¹ role by insulating the Indian subcontinent from cold northerly winds blowing down from central
⁴² Eurasia, keeping the surface temperatures high there during summer (see Boos and Kuang (2010)
⁴³ and Ma et al. (2014)).

⁴⁴ The other side of the contrast – the relatively cool waters of the northern Indian Ocean (NIO) –
⁴⁵ has been less explored. Privé and Plumb (2007b) compared the monsoons in simulations with their
⁴⁶ idealized atmospheric model forced by uniformly warm sea surface temperatures (SSTs) and by
⁴⁷ an SST profile that has a meridional gradient, and found that a meridional SST gradient promotes a
⁴⁸ cross-equatorial monsoon circulation. This picture was complicated, however, because the land in
⁴⁹ their idealized set-up is cooled by zonal winds coming from the colder waters adjacent to the land,
⁵⁰ damping the thermal contrast and hence the monsoon circulation (see also Chou et al. (2001)).
⁵¹ Privé and Plumb were able to strengthen the monsoon in their model by adding “walls” around the
⁵² continent to insulate it from these sea-breezes.

⁵³ While this provided a first indication of the relationship between the NIO and the monsoon cir-
⁵⁴ culation, it was highly idealized and did not consider feedbacks between the monsoonal winds and
⁵⁵ the SSTs. Webster and co-authors have suggested that the monsoon acts as a self-regulating sys-

tem (Loschnigg and Webster (2000); Webster et al. (2002); Chirokova and Webster (2006)), with strong monsoonal winds driving southward ocean heat transport (OHT) in the NIO, cooling the waters adjacent to the Indian subcontinent and hence damping the monsoon. This can be seen in observations, as the surface winds are southwesterly over the NIO in the summer and southeasterly south of the equator (arrows in Figure 1). This circulation pattern drives southward Ekman flow in the NIO’s mixed-layer, transporting heat into the southern hemisphere and potentially cooling the SSTs of the NIO. The heat transport can be inferred from the contours in Figure 1, which show the flux of heat from the atmosphere into the ocean. Developing a better understanding of the connection between OHT and monsoon circulations is the primary aim of this study.

The role of the Indian Ocean in cross-equatorial heat transport, but perhaps not monsoon dynamics, has been appreciated as far back as at least Levitus (1987) (see also Lee and Marotzke (1998)). Levitus hypothesized that the Ekman response to near surface equatorial winds in the Indian Ocean resulted in southward cross-equatorial heat transport in the boreal summer, which reversed in the winter. Ideas that describe the dynamical process involved, those of the Cross Equatorial Cell, are developed in McCreary et al. (1993), whose model was adapted by Loschnigg and Webster (2000) and Chirokova and Webster (2006).

Separate from the question of monsoons, the relationship between the zonal-mean atmospheric circulation and OHT has been investigated in a number of recent studies. It has been shown that including interactive OHT in idealized models substantially damps the Hadley circulation (Clement (2006); Levine and Schneider (2011); Singh et al. (2017)), as well as meridional shifts of the intertropical convergence zone (ITCZ, Green and Marshall (2017); Schneider (2017); though note that Clement (2006) found that OHT increases the amplitude of the seasonal migration of the ITCZ). The reason for this is that, because of its small gross moist stability, the tropical atmosphere is an inefficient transporter of energy (Held 2001). By contrast, the wind-driven subtropical

80 cells in the ocean efficiently transport energy away from the equator because of the large surface
81 temperature difference between the tropics and subtropics, which is mapped onto the vertical via
82 subduction (Klinger and Marotzke (2000); Held (2001); Czaja and Marshall (2005); Green and
83 Marshall (2017)). Hence including interactive OHT means that much less energy needs to be
84 transported to high latitudes by the atmosphere. These studies have focused on the zonal-mean
85 perspective, but similar considerations would be expected to apply to zonally-localized perturba-
86 tions, such as monsoons, with the caveat that we do not yet have a good understanding of what
87 controls the partitioning between zonal and meridional energy transports.

88 Putting these results together, coupling to the ocean has a number of competing effects on mon-
89 soonal circulations, potentially strengthening them by enhancing land-sea temperature gradients
90 and potentially weakening them by cooling the waters adjacent to land masses and by reducing
91 the energetic requirements on the cross-equatorial atmospheric circulation. Motivated by the geo-
92 graphic setting of the South Asian monsoon, in this study we take a first step towards untangling
93 the effects of ocean dynamics on monsoon circulations by investigating how the monsoon in a
94 moist, gray radiation atmospheric general circulation model (GCM) is affected by coupling the
95 GCM to a slab ocean with an interactive representation of OHT. The parameterization includes
96 an ocean stratification parameter that can be varied to directly control the strength of the OHT,
97 allowing us to systematically investigate the influence of OHT on the monsoon. We have also
98 performed sensitivity experiments without land and with the OHT fixed at its annual-mean value
99 to separate zonally-asymmetric effects from zonal-mean effects and to cut the coupling between
100 OHT and the monsoonal circulation.

101 We note that our focus is primarily on seasonal-means monsoon and not on monsoonal vari-
102 ability. Work with observations and with comprehensive models has demonstrated a strong link
103 between monsoon variability and SSTs; for instance, colder SSTs in the Bay of Bengal precede

¹⁰⁴ “breaks” in the South Asian monsoon, periods when the rains are muted, by about a week (e.g.,
¹⁰⁵ Vecchi and Harrison (2002); Schott et al. (2009)). However this kind of variability is unlikely to
¹⁰⁶ be well represented in our model, and our focus is instead on the seasonal-mean state of the mon-
¹⁰⁷soon, which the model can be expected to represent, at least in an idealized sense, and on the more
¹⁰⁸ general question of the relationship between the zonally-asymmetric atmospheric circulations and
¹⁰⁹ OHT.

¹¹⁰ The model and the simulations we have performed are described in more detail in the next
¹¹¹ section. In section 3 we investigate how the monsoon in our model is affected by coupling with
¹¹² the OHT, including how it is affected by varying the strength of the OHT and by fixing the OHT at
¹¹³ its annual-mean value. In section 4 we compare the model with more realistic coupled models to
¹¹⁴ assess how relevant our results may be for the South Asian monsoon and in section 5 we present
¹¹⁵ the results of experiments without land. We end with conclusions in section 6.

¹¹⁶ **2. Model Description and Simulations**

¹¹⁷ The model consists of the idealized moist GCM first described by Frierson et al. (2006), coupled
¹¹⁸ to a slab ocean with an idealized representation of OHT by the subtropical cells.

¹¹⁹ *a. The Moist GCM*

¹²⁰ The GCM solves the primitive equations on the sphere and uses gray radiative transfer. The
¹²¹ long-wave optical depth, τ , is specified to approximate the effects of atmospheric water vapor
¹²² (Frierson et al. 2006):

$$\tau(p, \phi) = \tau_0 \left[f_l \left(\frac{p}{p_s} \right) + (1 - f_l) \left(\frac{p}{p_s} \right)^4 \right], \quad (1)$$

¹²³ where p is pressure, ϕ is latitude, p_s is the surface pressure and the linear term is included to
¹²⁴ reduce stratospheric relaxation times (f_l is set to 0.1). τ_0 is the optical depth at the surface, and

¹²⁵ takes the form

$$\tau_0(\phi) = \tau_{0e} + (\tau_{0p} - \tau_{0e})\sin^2\phi, \quad (2)$$

¹²⁶ with τ_{0e} the surface value at the equator and τ_{0p} the surface value at the pole. These are set to 7.2
¹²⁷ and 1.8, respectively (O’Gorman and Schneider 2008). The solar insolation has an annual cycle,
¹²⁸ but no diurnal cycle, and is calculated as (see chapter 2 of Hartmann (2016)):

$$S_0 = \frac{S_c}{\pi} [h_0 \sin\phi \sin\delta + \cos\phi \cos\delta \sin h_0], \quad (3)$$

¹²⁹ where the solar constant S_c is set to 1360 W m^{-2} ; h_0 is the longitude of the subsolar point at sunrise
¹³⁰ and sunset relative to its position at noon; and δ is the declination, calculated using an obliquity of
¹³¹ 23.45° , a 360 day year and assuming that Earth’s orbit is perfectly circular. The albedo is fixed at
¹³² 0.38 and absorption of solar radiation by the atmosphere is modelled by calculating the downward
¹³³ shortwave flux at a given pressure level as $S = S_0 \exp(-\tau_s(p/p_s)^2)$, with τ_s fixed at 0.22, as used
¹³⁴ by O’Gorman and Schneider (2008).

¹³⁵ The model includes the simplified Betts-Miller (SBM) convection scheme of Frierson (2007),
¹³⁶ with a convective relaxation time-scale τ_{SBM} of 2 hours and a reference relative humidity RH_{SBM}
¹³⁷ = 0.7, and the boundary layer scheme is the one used by O’Gorman and Schneider (2008). In
¹³⁸ each experiment the model was integrated for eight years at T85 truncation (corresponding to a
¹³⁹ resolution of roughly 1.4° by 1.4° on a Gaussian grid) with 30 vertical levels extending up to
¹⁴⁰ 16hPa. Averages were taken over the last seven years of each simulation.

¹⁴¹ *b. Interactive OHT parameterization*

¹⁴² OHT can be represented as the product of a meridional overturning circulation and an energy
¹⁴³ contrast (Held (2001); Czaja and Marshall (2005))

$$q_O = c_{p,o} \Phi \Delta T, \quad (4)$$

144 where $c_{p,o}$ is the heat capacity of seawater, Φ is the overturning mass transport streamfunction
 145 and ΔT is the temperature difference across the upper and lower branches of the overturning cir-
 146 culation, i.e., between the top and base of the subtropical cells. This can also be thought of as
 147 the surface temperature difference between the deep tropics and the latitude of subduction, with
 148 typical values of 5-10K (Klinger and Marotzke 2000).

149 In the tropics, oceanic mass transport is mostly set by Ekman mass transport, allowing us to
 150 approximate the OHT as

$$q_O(\phi, \lambda) \approx ac_{p,o} \cos \phi \frac{\tau(\phi, \lambda)}{f(\phi)} \Delta T, \quad (5)$$

151 where λ is longitude, a is the radius of the Earth, τ is the wind stress and f is the Coriolis parame-
 152 ter. The interactive OHT parameterization assumes that heat is only transported via equation 5, and
 153 only calculates the OHT for latitudes between ϕ_1 , the latitude at which the surface winds change
 154 from westerly to easterly in the southern hemisphere, and ϕ_2 , the latitude at which the surface
 155 winds change from easterly to westerly in the northern hemisphere. $c_{p,o}$ is set to $3900 \text{ J kg}^{-1} \text{ K}^{-1}$
 156 and, importantly, ΔT is left as a free parameter to be specified.

157 This parameterization is similar to the scheme used by Klinger and Marotzke (2000) and Levine
 158 and Schneider (2011), except that their scheme uses surface quantities, so that the OHT is calcu-
 159 lated from the surface wind and temperature fields, with no free parameters. Here we specify ΔT
 160 directly in order to systematically investigate how the strength of the OHT impacts the monsoon,
 161 as larger ΔT values result in more heat being transported southwards in the summer.

162 As in Levine and Schneider (2011), we apply a Gaussian smoothing filter when calculating the
 163 divergence of the heat flux to avoid issues with f going to zero at the equator:

$$(\nabla \cdot q_O)' = \int_{\phi_1}^{\phi_2} \frac{1}{a \cos \phi} (\nabla \cdot q_O) P(\phi, \phi') d\phi', \quad (6)$$

¹⁶⁴ where

$$P(\phi, \phi') = \frac{1}{Z} \exp\left(\frac{-(\phi' - \phi)^2}{2s^2}\right), \quad (7)$$

¹⁶⁵ with Z chosen such that the integral of P from ϕ_1 to ϕ_2 is equal to one and s a half-width, which is
¹⁶⁶ set to 7° .

¹⁶⁷ Two drawbacks of this scheme are that the effective stability, ΔT , is the same at all locations
¹⁶⁸ and that the depth of the thermocline is fixed. For example, surface temperatures will warm where
¹⁶⁹ there is convergent Ekman mass flux, but in a more realistic model this would cause the ther-
¹⁷⁰ mocline to deepen, with little warming of the surface waters. As such, we compare our results
¹⁷¹ with a simulation which uses the “1.5-layer” parameterization of Ekman heat transport by Codron
¹⁷² (2012), though we have excluded diffusive heat transport and again only focus on heat transport
¹⁷³ in the tropics. In this scheme the temperature of the return flow, T_d is diagnosed from the surface
¹⁷⁴ temperature as

$$T_d = \alpha T_s + (1 - \alpha) T_0, \quad (8)$$

¹⁷⁵ where T_s is the surface temperature, T_0 is a reference temperature, here taken to be 273.15K,
¹⁷⁶ and ΔT is now equal to $T_s - T_d$. α varies linearly from 1/3 for purely divergent flow to 1 for
¹⁷⁷ purely convergent flow. This results in an effective stability that is large (up to about 15K) where
¹⁷⁸ there is divergence and small (~ 0 K) where there is convergence. Codron showed that, with these
¹⁷⁹ parameter values, the 1.5-layer scheme produces a reasonable representation of the climatology
¹⁸⁰ and seasonal cycle of SSTs when coupled to a comprehensive atmospheric GCM.

¹⁸¹ The depth of the ocean slab is fixed at 24m in all simulations. Donohoe et al. (2014) found
¹⁸² that coupling the AM2.1 GCM to a 24m slab ocean produces a climate with a reasonable seasonal
¹⁸³ migration of the ITCZ compared with observations, and also a reasonable annual-mean Hadley
¹⁸⁴ circulation and meridional distribution of precipitation.

“Land” is added to the model by reducing the mixed-layer depth to 0.5m and setting the ocean heat flux divergence to zero between 100° - 235° E and 15° - 40° N. This provides an infinite supply of moisture for the monsoonal circulation and also means that the global integral of q_o is not always zero. So there may be net OHT from the northern hemisphere into the southern hemisphere, even for conditions that are otherwise hemispherically-symmetric, however we find that in the annual-mean the ITCZ is very close to the equator in all of our simulations (not shown).

The geometry of our set-up is illustrated in Figure 2.

c. Simulations

We have performed three sets of simulations with the model, motivated by our aim of untangling the competing effects of OHT on the monsoon. The main set includes both land and the interactive OHT, with ΔT varied from 0K (i.e., no OHT) to 15K. In a second set of simulations the OHT at each grid point is fixed at its annual-mean value from the first set of simulations, eliminating the coupling between OHT and the monsoonal circulation but maintaining the annual-mean effects of OHT. The third set include the interactive OHT but not the land, with ΔT again varied from 0K to 15K. Comparing these simulations with the first set of simulations allows the impacts of the OHT on the zonal-mean circulation to be separated out.

3. The Relationship Between OHT and the Model’s Monsoon

a. Comparing Simulations With and Without OHT

We begin by comparing the monsoons in a simulation without OHT and a simulation with $\Delta T = 10$ K, which is one of our more realistic simulations (see sections 3b and 4). Figure 3 shows the summertime¹ precipitation and surface winds (top panels), the summertime surface moist static

¹“Summer” is defined as the 90 days with the highest insolation over the land and “winter” as the 90 days with the least insolation over the land.

206 energy (middle panels) and the summertime ocean heat flux divergence for the interactive case
207 (bottom right panel). The surface moist static energy is calculated as $c_p T + L_v q_v$, where c_p is the
208 specific heat capacity of dry air, T is the temperature at the lowest model level, L_v is the latent heat
209 of vaporization of liquid water and q_v is the specific humidity at the lowest model level.

210 Without OHT, the ITCZ is slightly north of the equator, at about 5°N in the zonal-mean, and there
211 is also a weak precipitation maximum just south of the continent. The surface MSE is relatively
212 uniform throughout the tropics, with the largest values on the southern edge of the continent. The
213 winds resemble the observations (Figure 1), being southeasterly up to about 5°N and then swinging
214 around to be southwesterly between 5°N and 20°N, though the winds north of 5° are weak.

215 In the simulation with OHT there is much clearer evidence of a monsoon, with the highest
216 precipitation over the southern edge of the continent, at about 17°N. The winds again resemble
217 the observations, and are stronger between 5°N and 20°N than in the no OHT case. The surface
218 MSE is generally smaller than in the simulation without OHT, because the OHT parameterization
219 redistributes heat to the subtropics (see also Clement (2006)), and there is a sharper maximum in
220 MSE over the continent, resulting in a larger land-ocean contrast in low-level MSE. Panel e) of
221 Figure 3 shows that the ocean transports heat southwards across the equator, as well as from the
222 tropics into the subtropics of the Northern Hemisphere.

223 Figure 4 compares the seasonal cycles in precipitation (top panels) and surface MSE (bottom
224 panels) in these simulations, with values averaged over the land sector. Without OHT the maxi-
225 mum precipitation varies smoothly over the course of the year, following the maximum insolation,
226 though there is increased precipitation just south of the land in the late spring and summer months.
227 The MSE shows a similar progression, and the largest MSE is in the summer and early fall because
228 of the larger warming of the land.

229 The seasonal cycle of precipitation is less regular when OHT is included, and the maximum
230 precipitation is weaker than in the simulation without OHT (panel c). Both the precipitation and
231 the maximum MSE jump to the warmer hemisphere during the transition seasons so that, as in
232 Clement (2006), the seasonal migration of the ITCZ is larger with OHT. The amplitude of the
233 seasonal cycle in MSE is larger in the Northern Hemisphere than in the Southern Hemisphere, as
234 the highest MSE values are found over the land in the summer months, while the lowest MSE
235 values are over the land in the winter months. This is discussed further in section 5.

236 *b. Varying ΔT*

237 The effects of varying the strength of the OHT on the surface climate of the model are summa-
238 rized in Figure 5. As ΔT is increased the tropical SSTs in the land sector cool and the meridional
239 SST gradient is reduced (panel a). However the land-ocean SST contrast increases dramatically,
240 going from about 0.2K to 1.5K as ΔT is increased from 0K to 15K. The MSE has a similar
241 progression (panel b), though the profile is smoother, without such a sharp jump across the land-
242 ocean boundary (panel d). A secondary MSE maximum develops in the southern hemispheres of
243 the experiments with large ΔT . The smoothness of the MSE reflects smoother profiles of near-
244 surface air temperature and specific humidity. We hypothesize that the near-surface air temper-
245 ature and specific humidity do not track the SSTs more closely because the air-sea temperature
246 difference must vary in order for the turbulent fluxes of sensible and latent heat to balance the
247 convergence/divergence of OHT.

248 The ITCZ is close to 5°N in the 0K and 2.5K simulations, before jumping over the land in the
249 5K simulation. This appears to be an intermediate case, as the ITCZs in the 10K and 15K cases are
250 very similar to each other. The OHT is also similar in these two simulations (panel e), suggesting
251 that it may saturate for large enough ΔT . Privé and Plumb (2007a) showed that precipitation

252 maxima will occur slightly equatorward of maxima in the surface MSE, where the meridional
253 gradient in surface MSE (to which the vertical wind shear is proportional) is largest. Although the
254 maximum MSE in the 0K and 2.5K cases is over the land, there are also MSE maxima near 5°N
255 in these simulations.

256 Figure 6 plots the zonal-winds in these simulations in black contours and the mean meridional
257 circulation (MMC) in the red contours. The MMC is calculated as $\frac{1}{g} \int_{ps}^P \bar{v}(p', \phi) dp'$, where an
258 overbar denotes an average over the land sector (Note that because the average is taken over a
259 limited sector, this circulation does not necessarily conserve mass). The overturning circulation
260 expands and weakens as ΔT is increased, while the vertical shear in the zonal wind, which is often
261 taken as a proxy for the strength of the monsoonal circulation (Webster and Yang 1992), increases.
262 This is primarily due to a strengthening of the easterlies near the tropopause. For larger ΔT a jump
263 in the near-surface meridional circulation develops just north of the equator because it is difficult
264 for the low-level return flow of the Hadley Circulation to cross the equator when the equatorial
265 surface temperature gradient is weak (Pauluis 2004).

266 The round markers in Figure 7 quantify these changes by showing the maximum vertical zonal
267 wind shear ($u(850\text{hPa}) - u(250\text{hPa})$) between the equator and 20°N as a function of ΔT in panel a)
268 and the minimum (i.e., the most negative) values of the MMC as a function of ΔT in panel b). The
269 zonal wind shear increases slightly when going from 0K to 2.5K, then jumps at 5K and increases
270 roughly linearly as ΔT is increased further. Comparing with panel c) of the Figure shows that
271 this progression closely tracks the changes in the MSE gradient. In an angular momentum (AM)
272 conserving flow the zonal-wind shear is proportional to the subcloud MSE gradient (Emanuel
273 1995) and, though the flow in these simulations is far from the AM-conserving limit (see below),
274 we believe that this argument is still relevant here.

Conversely, the strength of the MMC decreases roughly linearly from 0K to 10K and then increases slightly for $\Delta T = 15\text{K}$. The decrease over the first four simulations is expected from the discussion in the introduction: as ΔT is increased the atmosphere has to transport less energy across the equator and so the circulation slows down. A quantitative theory for the compensation between energy transport by the Hadley circulation and OHT is still lacking, however, and in particular requires a better understanding of how the gross moist stability of the tropical atmosphere is controlled (Singh et al. 2017).

Panel d) of Figure 7 shows the minimum absolute vorticity ($f + \bar{\zeta}$, where f is the Coriolis parameter and ζ is the relative vorticity) polewards of 7° during the summer of these simulations. The absolute vorticity vanishes in the upper troposphere of an AM-conserving flow and, although none of the simulations are close to this regime, there is a substantial decrease in the minimum absolute vorticity, from about $0.55 \times 10^{-5}\text{s}^{-1}$ to $0.41 \times 10^{-5}\text{s}^{-1}$ when going from $\Delta T = 10\text{K}$ to $\Delta T = 15\text{K}$. This step towards an AM-conserving flow is caused by the increased vertical wind shear, as the stronger upper-level easterlies shield the tropical circulation from baroclinic eddies originating at mid-latitudes (Bordoni and Schneider 2008). Since these eddies act as a drag on the mean flow, increased shielding may explain why the MMC strengthens in the $\Delta T = 15\text{K}$ case (Walker and Schneider 2006).

In summary, increasing ΔT both strengthens the monsoonal circulation by increasing the land-sea contrast and damps the monsoon because less heat needs to be carried across the equator by the atmosphere.

295 c. Specifying the OHT

The effects of the OHT on the monsoon come partly from the seasonal variations in the OHT and partly from the effects of the annual-mean OHT. Our second set of simulations separate these

298 out, as the OHT is fixed at the annual-mean profiles from the interactive experiments. The crosses
299 in the top panels of Figure 7 show that this increases the maximum zonal-wind shear and also the
300 MMC. The MSE gradient also increases (panel c), while the minimum absolute vorticity decreases
301 rapidly, so that the flow is approximately AM-conserving for $\Delta T = 10K$ and above (panel d).
302 While this transition to an AM-conserving regime will strengthen the flow somewhat, panel e) of
303 the Figure shows that in fact the MMC scales linearly with the OHT at the equator, so that the
304 energetic requirements on the Hadley circulation are the dominant control on its strength.

305 More insight into the effects of specifying the OHT on the monsoon comes from the left panels
306 Figure 8, which show the summer climate in the case with the OHT from the $\Delta T = 10K$ case. The
307 monsoon is stronger than in the corresponding case with interactive OHT, with stronger winds
308 and precipitation, as well as a larger land-sea MSE contrast. The shape of the winds means in
309 particular that the monsoon is strongest in the southeast corner of the continent. The reason for
310 this stronger monsoon can be seen by comparing panel e), which shows the OHT divergence
311 in this simulation, with panel e) of Figure 3. The annual-mean OHT is still southwards in the
312 land sector, but the ocean now converges heat at the latitudes of the south coast of the continent
313 ($15\text{-}20^\circ$), rather than diverging heat as it was in the interactive case. This warms the waters on
314 either side of the continent, so that the continent is not cooled as much by zonal breezes as it was
315 in the interactive case. This is reminiscent of how Privé and Plumb (2007b) found that adding
316 walls to their continent strengthened the monsoon by insulating it from zonal sea breezes (see
317 Introduction).

318 **4. Comparison with More Realistic Models**

319 The above results give an indication of how OHT might affect monsoon circulations, however
320 the idealized nature of our model puts into question the relevance of our results for the real atmo-

sphere. As a first way of assessing this relevance, the dashed red lines in Figure 7 show values from the simulation with the 1.5-layer parameterization. These generally lie between the $\Delta T = 5\text{K}$ and $\Delta T = 10\text{K}$ simulations, with the vertical wind shear closer to the 5K case and the MMC closer to the 10K case. Comparing the middle column with the right column of Figure 3 also demonstrates the similarities between the 1.5-layer simulation and the $\Delta T = 10\text{K}$ case. So even with ΔT allowed to vary with latitude in a realistic manner, OHT has a major impact on the monsoon circulation in this model.

Next, we investigate the seasonal cycles of SSTs and of the ocean heat budget in our simulations. Another drawback of the interactive OHT parameterization is that the mixed-layer depth (MLD) is kept fixed: in the real ocean changes in OHT do not necessarily lead to changes in SSTs, because the MLD may also deepen or shoal. Moreover, the circulation and temperature in the thermocline take time to adjust to different surface conditions, whereas this adjustment is instantaneous in both our simple parameterization and the 1.5-layer parameterization. These two deficiencies mean that our model misses any potential phase difference between changing surface winds and OHT-induced SST variations.

The heat budget for a volume of ocean water is

$$Q_S(t) = Q_O(t) + Q_F(t), \quad (9)$$

where Q_S is the change in heat stored in the volume:

$$Q_S(t) = a^2 \rho c_{p,0} \int_{MLD}^0 \int_{\phi_1}^{\phi_2} \int_{\lambda_1}^{\lambda_2} \frac{dT}{dt} \cos\phi d\lambda d\phi dz, \quad (10)$$

where ρ is the density of seawater and T is the depth-averaged temperature of the mixed-layer. Q_O is the OHT (q_O) integrated around the lateral boundaries of the volume, as well as heat fluxed through the bottom of the mixed-layer (which we ignore) and Q_F is the surface heat flux into the

341 water:

$$Q_F(t) = a^2 \int_{\phi_1}^{\phi_2} \int_{\lambda_1}^{\lambda_2} (Q_{SW} + Q_{LW} + Q_{LH} + Q_{SH}) \cos\phi d\lambda d\phi, \quad (11)$$

342 where Q_{SW} is the incoming solar radiation at the surface, Q_{LW} is the outgoing longwave radiation
343 at the surface, Q_{LH} is the surface latent heat flux and Q_{SH} is the surface sensible heat flux. Note
344 that if Q_F is fixed then changes in Q_O can be compensated either by changes in T or by changes
345 in the MLD and so since the MLD is fixed in our model changes in Q_O can only be compensated
346 by changes in T .

347 Figure 9a shows the heat budget for the ocean off the coast of the continent (100° to 235°E and
348 0 to 15°N) for the simulation with land and $\Delta T = 10K$ in black, and for the 1.5-layer simulation
349 in red. In both simulations, the ocean carries heat north across the equator in winter and south in
350 summer, while it is warmed by the surface fluxes in summer and cooled in the winter. The largest
351 surface fluxes are in the spring and in the fall because the strong monsoon winds in the summer
352 lead to enhanced evaporative cooling over the ocean. These terms produce a seasonal cycle in the
353 SSTs of $\sim 4K$ in the $\Delta T = 10K$ case (solid line in Figure 9b) and $\sim 3K$ in the 1.5-layer simulation
354 (dotted red line), with the warmest SSTs in both cases coming in the fall when the OHT and the
355 monsoonal winds are weaker.

356 These results agree qualitatively with previous studies of the heat budget of the NIO, though
357 there are some notable differences. Comparing with Figure 3 of Chirokova and Webster (2006),
358 the seasonal cycles of the OHT and of the surface fluxes in our simulations are similar to their
359 modelled NIO, except that the OHT is generally larger than the surface fluxes in their simulations
360 whereas the reverse is the case in our simulations (see also Figure 21 of Lee and Marotzke (1998)),
361 though we note that because of our idealized set-up we are not averaging over the same geometries.
362 The other major difference is that Chirokova and Webster (2006) and Lee and Marotzke (1998)

³⁶³ both find that Q_F is almost zero during the summer and early fall, because increased cloudiness
³⁶⁴ reduces the solar radiation absorbed by the surface (as a reminder, there are no clouds in our
³⁶⁵ model) and because of stronger evaporative cooling than in our simulations, caused by stronger
³⁶⁶ monsoonal winds. The large reduction in Q_F in the summer means that the warmest SSTs in the
³⁶⁷ NIO are actually in April and May (dashed black line in Figure 9b), rather than in the fall.

³⁶⁸ Babu et al. (2004) showed that the MLD in the NIO is shallowest in February and March, which
³⁶⁹ contributes to the warm SSTs in the spring, and then deepens over the course of the summer due
³⁷⁰ to mixing caused by the monsoonal winds. The mixed-layer shoals rapidly again in the fall at
³⁷¹ the end of the monsoon season and then deepens in the winter months. The gradual deepening
³⁷² of the mixed-layer during the summer will damp the cooling of the NIO SSTs by OHT during
³⁷³ the summer months, but on the whole we believe that our model underestimates the cooling of
³⁷⁴ SSTs by OHT, and the amplitude of the seasonal cycle of SSTs in the NIO is smaller than in our
³⁷⁵ model (Figure 9b). So although there are differences between the heat budgets in our model and
³⁷⁶ in the more realistic models of Lee and Marotzke (1998) and Chirokova and Webster (2006) due
³⁷⁷ to the fixed mixed-layer depth and the lack of clouds in our model, we believe that our model
³⁷⁸ qualitatively captures the impact of OHT on SSTs equatorward of subtropical continents, and that
³⁷⁹ the effects of any phase lag are minor.

³⁸⁰ 5. Zonal-Mean Effects

³⁸¹ The behavior discussed in section 3 comes from the monsoon generated over the land, but also
³⁸² from the zonal-mean effects of the interactive OHT. We use our third set of experiments – with
³⁸³ interactive OHT but no land – to investigate how the interactive OHT affects the zonal-mean
³⁸⁴ circulation of the model.

385 The triangles in Figure 7a show that excluding the land reduces the vertical zonal wind shear by
386 roughly half, though this still increases as ΔT is increased and the MSE gradient also strengthens
387 (panel b). So, even without the land the southward energy transport by the ocean still produces
388 a monsoon-like circulation. The MMC is very similar with and without land (Figure 7b), as it is
389 mostly determined by the OHT (section 3.3).

390 These experiments, together with the fixed OHT experiments, can also be used to understand the
391 seasonal cycles in Figure 4. In the simulation without land and with $\Delta T = 10K$ there are actually
392 three maxima in the precipitation (Figure 10a), one close to the equator and one further polewards
393 in each hemisphere, with all three shifting gradually over the course of the year. A double-ITCZ
394 structure is expected because the OHT and the heat transport by the atmosphere result in the net
395 energy input to the deep tropics being negative (Clement (2006); Bischoff and Schneider (2016)),
396 while the peak at the equator is caused by rising motion as the meridional circulation jumps over
397 the equator (not shown).

398 The fixed OHT experiment resembles the original Hovmuller diagrams, but with the features
399 exaggerated (Figure 10c and f). In the winter there is very little precipitation in the northern hemi-
400 sphere and a strong maximum in precipitation at about -15°S . A strong maximum appears in the
401 northern hemisphere over the land in the spring, while the maximum in the southern hemisphere
402 weakens and gradually shifts to the north, joining the strong peak over the land in the late sum-
403 mer. During the fall the maximum slowly migrates southwards, before jumping further south once
404 winter sets in.

405 These jumps are primarily caused by strong surface winds blowing south off the continent in the
406 winter (Figure 8b). Because the continent is very cold in the winter, these winds cool the oceans
407 to the south of the continent, creating a strong meridional MSE gradient compared to the warmer
408 waters of the southern hemisphere (Figure 8d; note that the MSE near the equator is colder than

409 in the summer). These winds die down in the spring as the land – and the oceans to either side
410 of it – warm up, rapidly reducing the MSE gradient and causing a strong MSE and precipitation
411 maximum to develop over the continent. At the same time, the precipitation maximum in the
412 south migrates northwards, following the peak insolation, until it merges with the maximum over
413 the land. In the fall the land cools and the MSE maximum gradually migrates southwards until the
414 strong winds pick up again, rapidly cooling the ocean and causing the jump to the strong southern
415 precipitation maximum during winter.

416 We have performed an additional experiment without land and with the OHT fixed at its annual-
417 mean value from the no-land $\Delta T = 10\text{K}$ experiment. This is similar to the fixed OHT with land,
418 though the precipitation maxima are weaker (Figure 10b). The MSE is smallest in the transition
419 months (Figure 10e), when it has a minimum near the equator because the atmosphere and ocean
420 transport heat to higher latitudes, resulting in a double-ITCZ. In the summer and winter, the atmo-
421 sphere transfers heat into the tropics, so that they gain energy in the net (not shown) and there is a
422 single ITCZ.

423 Together, these can explain the features seen in Figure 4. The jumps in the precipitation max-
424 imum and in the MSE maximum come about because of the rapid warming and cooling of the
425 continent, but at the same time the interactive OHT promotes a double ITCZ, as there is net energy
426 transport out of the deep tropics.

427 6. Conclusion

428 In this study we have investigated the monsoon in an idealized model consisting of the widely
429 used gray-radiation atmospheric GCM, coupled to an idealized parameterization of ocean heat
430 transport by the subtropical cells. The OHT parameterization includes a parameter, ΔT , which can

⁴³¹ be used to vary the strength of the OHT, allowing us to systematically investigate the impact of
⁴³² OHT on the monsoon in this model.

⁴³³ Without OHT the monsoon in our model is weak, because the land surface is not protected from
⁴³⁴ cold winds coming either from further north or from the east and west of the land (see also Chou
⁴³⁵ et al. (2001) and Privé and Plumb (2007b)). However, by increasing ΔT sufficiently we are able
⁴³⁶ to create a reasonable monsoon circulation because the waters south of the land cool during the
⁴³⁷ summer, creating a strong meridional MSE gradient. This includes increases in the vertical wind
⁴³⁸ shear as ΔT is increased and in the precipitation over land, though the MMC weakens. The shear
⁴³⁹ strengthens because the meridional MSE gradient increases, while the MMC weakens because
⁴⁴⁰ the increased OHT means that the atmosphere is required to transport less heat across the equator
⁴⁴¹ (Clement (2006); Singh et al. (2017)). For $\Delta T = 15\text{K}$ the vertical shear is strong enough to start
⁴⁴² pushing the flow towards an angular momentum-conserving regime. Fixing the OHT at its annual-
⁴⁴³ mean value results in the OHT warming the waters zonally-adjacent to the land, rather than cooling
⁴⁴⁴ them, as in the case with interactive OHT, but the waters south of the land are still cooled as there
⁴⁴⁵ is southwards OHT in the land sector (Figure 8e). This increases the MSE gradient compared
⁴⁴⁶ to the interactive case, resulting in a stronger monsoon circulation, which causes the flow in the
⁴⁴⁷ simulations with $\Delta T = 10\text{K}$ and above to be in an AM-conserving regime. Comparisons with
⁴⁴⁸ a simulation that uses the 1.5-layer parameterization of Codron (2012) and with the results of
⁴⁴⁹ Chirokova and Webster (2006) and Lee and Marotzke (1998) suggest that our most realistic cases
⁴⁵⁰ are the $\Delta T = 5\text{K}$ and $\Delta T = 10\text{K}$ cases and that, if anything, our model underestimates the effects
⁴⁵¹ of OHT on SSTs south of subtropical continents.

⁴⁵² Combining the original experiments with the fixed OHT experiments and the experiments with-
⁴⁵³ out land showed that the changes in the MMC are largely due to changes in the OHT, with the
⁴⁵⁴ MMC weakening as the OHT increased. By contrast, the presence of land and/or of a transi-

tion to an AM-conserving regime have minor impacts on the MMC, except insofar as they effect
the OHT. Finally, the seasonal cycle of precipitation in the interactive OHT simulations exhibits
jumps, as strong precipitation suddenly appears over the continent in the summer and in the south-
ern hemisphere during winter. These jumps are even clearer in the simulations with fixed OHT,
and are caused by strong winds blowing off the continent during the winter months, which cool
the waters south of the continent and set-up a strong MSE maximum in the southern hemisphere.
When the land warms up sufficiently these winds stop and the waters north of the equator warm
up quickly, while an MSE maximum develops over the land. When the land starts to cool in the
fall the MSE maximum at first gradually shifts southwards, until the strong winds reappear and
the maximum MSE jumps southwards. The jumps are clearer in the simulations without the inter-
active OHT because removing the link between OHT and the surface winds reduces the variability
of the precipitation and also makes the model less likely to have a double-ITCZ.

These results have been obtained with an idealized model, but demonstrate the substantial impact
OHT can have on the monsoonal circulation, both through the zonal-mean effect of the atmosphere
needing to transport less heat across the equator and through the local effect of creating a stronger
meridional MSE gradient. Work with more comprehensive models, which include clouds and
realistic topography, is required to further assess the impact these effects have on the South Asian
monsoon, which is the original motivation for our study. Furthermore, as has been noted in several
previous studies, a theory for the compensation between the ocean and the atmosphere is required
in order to quantitatively predict how the overturning circulation is affected by the increased OHT,
particularly a theory for how the gross moist stability of the tropical atmosphere is affected.

The Indian subcontinent seems to be ideally situated to develop a strong monsoon, being in-
sulated from cold winds blowing down from Eurasia by the Himalayas to the north, while to the
south the northern Indian Ocean transports heat southwards, cooling the SSTs off the coast of India

479 and further enhancing the meridional MSE gradient. Previous studies have mostly focused on the
480 effects of the Himalayas and the Tibetan plateau on the monsoon, and have used either prescribed
481 SSTs (e.g., Boos and Kuang (2010); Ma et al. (2014)) or slab oceans with Q -fluxes added to ensure
482 the slab's SSTs closely match the observed climatological-mean SSTs (Park et al. 2014); however
483 a realistic representation of OHT in the Northern Indian Ocean is required for a complete picture
484 of the South Asian monsoon.

485 *Acknowledgment.* We thank Peter Webster and Tim Cronin for helpful discussions, and three
486 anonymous reviewers, whose comments substantially improved the manuscript. Nicholas Lutsko
487 was partly supported by NSF grant AGS-1623218, “Collaborative Research: Using a Hierarchy of
488 Models to Constrain the Temperature Dependence of Climate Sensitivity”, and Brian Green was
489 partly supported by a grant from NOAA.

490 References

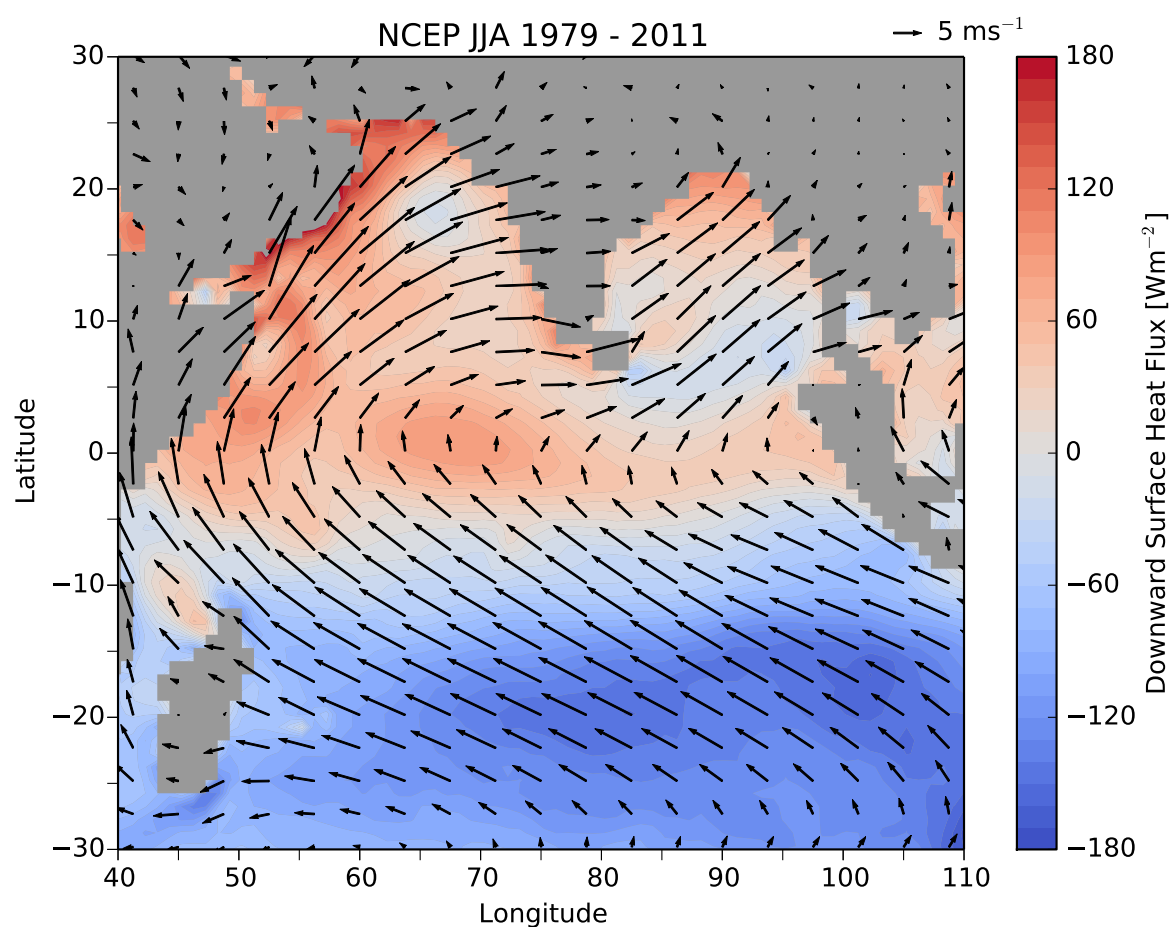
- 491 Babu, K. N., R. Sharma, N. Agarwal, A. V. K., and W. R. A., 2004: Study of the mixed layer depth
492 variations within the north indian ocean using a 1d model. *Journal of Geophysical Research: Oceans*, **109** (C8).
- 493 Bischoff, T., and T. Schneider, 2016: The equatorial energy balance, itcz position, and double itcz
494 bifurcations. *Journal of Climate*, **29** (15), 2997–3013.
- 495 Boos, W. R., and Z. Kuang, 2010: Dominant control of the south asian monsoon by orographic
496 insulation versus plateau heating. *Nature*, **463** (23), 218–222.
- 497 Bordoni, S., and T. Schneider, 2008: Monsoons as eddy-mediated regime transitions of the tropical
498 overturning circulation. *Nature Geoscience*, **1** (23), 515–519.

- 500 Chirokova, G., and P. J. Webster, 2006: Interannual variability of indian ocean heat transport.
- 501 *Journal of Climate*, **19** (6), 1013–1031.
- 502 Chou, C., J. D. Neelin, and H. Su, 2001: Ocean-atmosphere-land feedbacks in an idealized mon-
- 503 soon. *Quarterly Journal of the Royal Meteorological Society*, **127** (15), 1869–1891.
- 504 Clement, A. C., 2006: The role of the ocean in the seasonal cycle of the hadley circulation. *Journal*
- 505 *of the Atmospheric Sciences*, **63** (23), 3351–3365.
- 506 Codron, F., 2012: Ekman heat transport for slab oceans. *Climate Dynamics*, **38** (1), 379–389.
- 507 Czaja, A., and J. Marshall, 2005: The partitioning of poleward heat transport between the atmo-
- 508 sphere and ocean. *Journal of the Atmospheric Sciences*, **63**, 1498–1511.
- 509 Donohoe, A., D. M. W. Frierson, and D. S. Battisti, 2014: The effect of ocean mixed layer depth
- 510 on climate in slab ocean aquaplanet experiments. *Climate Dynamics*, **43** (3), 1041–1055.
- 511 Emanuel, K. A., 1995: On thermally direct circulations in moist atmospheres. *Journal of the*
- 512 *Atmospheric Sciences*, **52** (15), 1529–1534.
- 513 Frierson, D. M. W., 2007: The dynamics of idealized convection schemes and their effect on the
- 514 zonally averaged tropical circulation. *Journal of the Atmospheric Sciences*, **64** (23), 1959–1976.
- 515 Frierson, D. M. W., I. M. Held, and P. Zurita-Gotor, 2006: A gray-radiation aquaplanet moist gcm.
- 516 part i: Static stability and eddy scales. *Journal of the Atmospheric Sciences*, **63** (23), 2548–2566.
- 517 Geen, F., F. H. Lambert, and G. K. Vallis, 2018: Regime change behavior during asian monsoon
- 518 onset. *Journal of Climate*, **31** (9), 3327–3348.
- 519 Green, B., and J. Marshall, 2017: Coupling of trade winds with ocean circulation damps itcz shift.
- 520 *Journal of Climate*, **30** (12), 4395–4411.

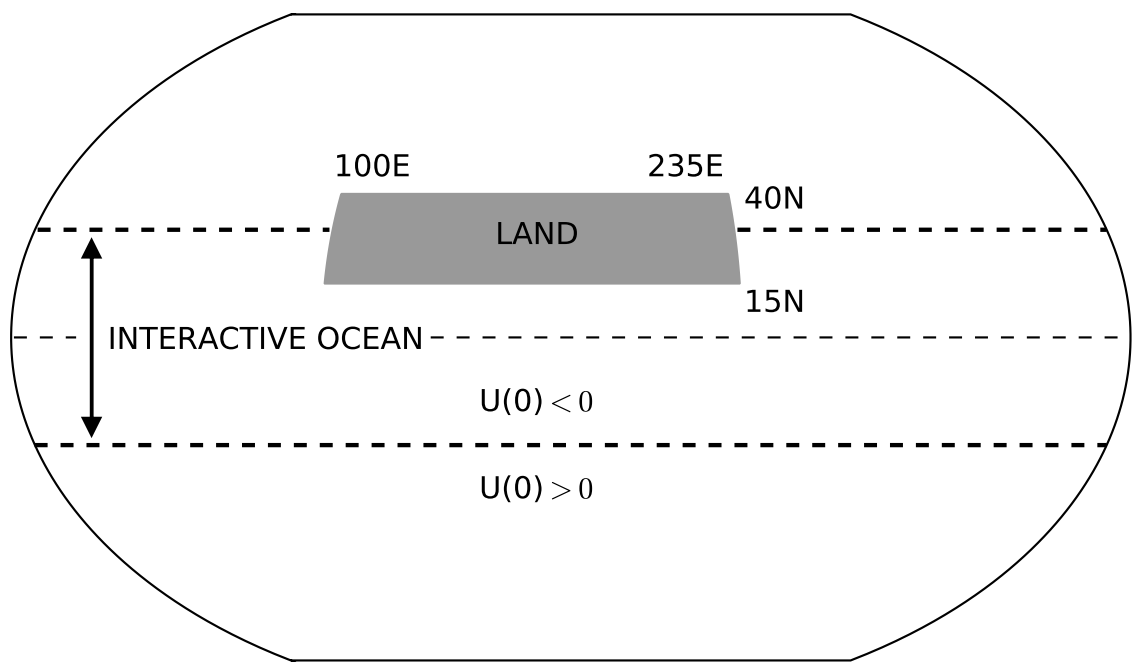
- 521 Hartmann, D. L., 2016: *Global Physical Climatology*. 2nd ed., Elsevier.
- 522 Held, I. M., 2001: The partitioning of the poleward energy transport between the tropical ocean
523 and atmosphere. *Journal of the Atmospheric Sciences*, **58**, 943–948.
- 524 Klinger, B. A., and J. Marotzke, 2000: Meridional heat transport by the subtropical cell. *Journal*
525 *of Physical Oceanography*, **30** (23), 696–705.
- 526 Lee, T., and J. Marotzke, 1998: Seasonal cycles of meridional overturning and heat transport of
527 the indian ocean. *Journal of Physical Oceanography*, **28** (23), 923–943.
- 528 Levine, X. J., and T. Schneider, 2011: Response of the hadley circulation to climate change in
529 an aquaplanet gcm coupled to a simple representation of ocean heat transport. *Journal of the*
530 *Atmospheric Sciences*, **68** (8), 769–783.
- 531 Levitus, S., 1987: Meridional ekman heat fluxes for the world ocean and individual ocean basins.
532 *Journal of Physical Oceanography*, **17** (23), 1484–1492.
- 533 Loschnigg, J., and P. J. Webster, 2000: A coupled oceanatmosphere system of sst modulation for
534 the indian ocean. *Journal of Climate*, **13** (104), 3342–3360.
- 535 Ma, D., W. R. Boos, and Z. Kuang, 2014: Effects of orography and surface heat fluxes on the
536 south asian summer monsoon. *Journal of Climate*, **27** (9), 6647–6659.
- 537 McCreary, J. P., P. K. Kundu, and R. L. Molinari, 1993: A numerical investigation of the dynamics,
538 thermodynamics and mixed layer processes in the indian ocean. *Progress in Oceanography*,
539 **31** (23), 181–244.
- 540 O’Gorman, P. A., and T. Schneider, 2008: The hydrological cycle over a wide range of climates
541 simulated with an idealized gcm. *Journal of Climate*, **21** (15), 3815–3832.

- 542 Park, H.-S., J. C. H. Chiang, and S. Bordoni, 2014: The mechanical impact of the tibetan plateau
543 on the seasonal evolution of the south asian monsoon. *Journal of Climate*, **25** (9), 2394–2407.
- 544 Pauluis, O., 2004: Boundary layer dynamics and cross-equatorial hadley circulation. *Journal of*
545 *the Atmospheric Sciences*, **61** (23), 1161–1173.
- 546 Plumb, R. A., and A. Y. Hou, 1992: The response of a zonally symmetric atmosphere to sub-
547 tropical thermal forcing: Threshold behavior. *Journal of the Atmospheric Sciences*, **49** (23),
548 1790–1799.
- 549 Privé, N. C., and R. A. Plumb, 2007a: Monsoon dynamics with interactive forcing. part i: Ax-
550 isymmetric studies. *Journal of the Atmospheric Sciences*, **64** (23), 1417–1430.
- 551 Privé, N. C., and R. A. Plumb, 2007b: Monsoon dynamics with interactive forcing. part ii: Impact
552 of eddies and asymmetric geometries. *Journal of the Atmospheric Sciences*, **64** (23), 1431–1442.
- 553 Schneider, T., 2017: Feedback of atmosphere-ocean coupling on shifts of the intertropical conver-
554 gence zone. *Geophysical Research Letters*, **44** (12), 11 644–11 653.
- 555 Schott, F. A., S.-P. Xie, and J. P. McCreary, 2009: Indian ocean circulation and climate variability.
556 *Reviews of Geophysics*, **47** (1).
- 557 Singh, M. S., Z. Kuang, and Y. Tian, 2017: Eddy influences on the strength of the hadley circula-
558 tion: Dynamic and thermodynamic perspectives. *Journal of the Atmospheric Sciences*, **74** (15),
559 467–486.
- 560 Vecchi, G. A., and D. E. Harrison, 2002: Monsoon breaks and subseasonal sea surface temperature
561 variability in the bay of bengal. *Journal of Climate*, **15** (1), 1485–1493.
- 562 Walker, C. C., and T. Schneider, 2006: Eddy influences on hadley circulations: Simulations with
563 an idealized gcm. *Journal of the Atmospheric Sciences*, **63** (15), 3333–3350.

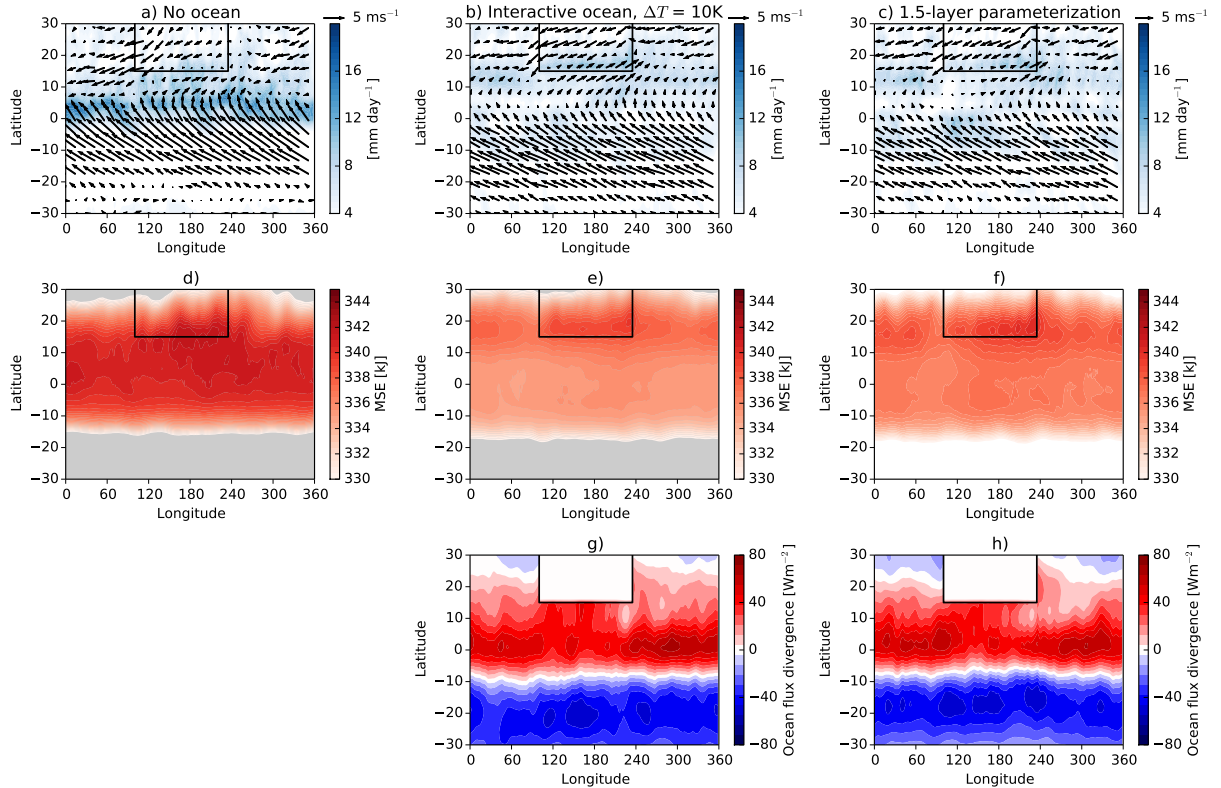
- 564 Webster, P. J., C. Clark, G. Cherikova, J. Fasulla, W. Han, J. Loschnigg, and K. Sahami, 2002:
- 565 The monsoon as a self-regulating coupled oceanatmosphere system. *International Geophysics*,
- 566 **83 (2)**, 198–219.
- 567 Webster, P. J., and S. Yang, 1992: Monsoon and enso: Selectively interactive systems. *Quarterly*
- 568 *Journal of the Royal Meteorological Society*, **118 (23)**, 877–926.
- 569 Zhai, J., and W. Boos, 2015: Regime transitions of cross-equatorial hadley circulations with zon-
- 570 ally asymmetric thermal forcings. *Journal of the Atmospheric Sciences*, **64 (23)**, 3800–3818.



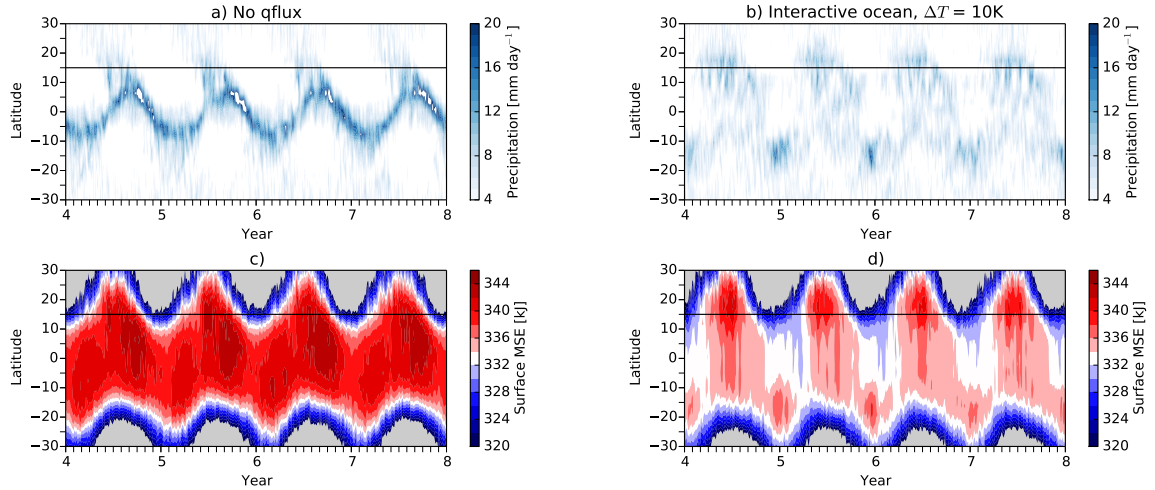
571 FIG. 1. Climatological June-July-August (JJA) downward energy flux at the ocean surface (contours) and
572 surface winds (arrows) from the NCEP reanalysis for the period 1979 to 2011.



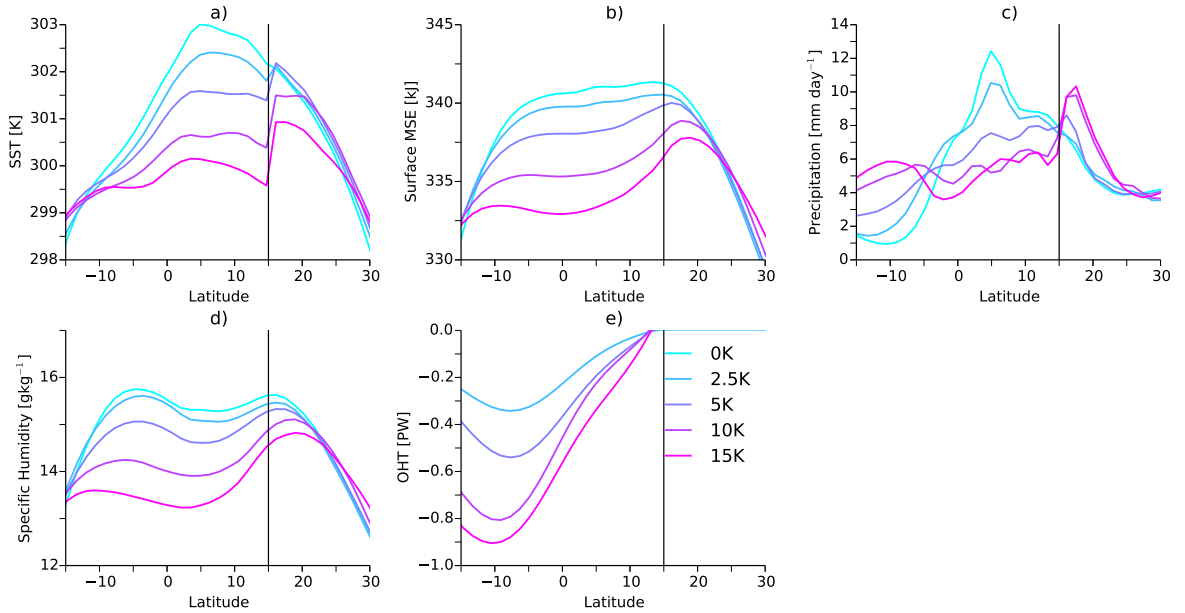
573 FIG. 2. Schematic of the model configuration used in the experiments. Note that the boundaries of the
574 interactive ocean move seasonally.



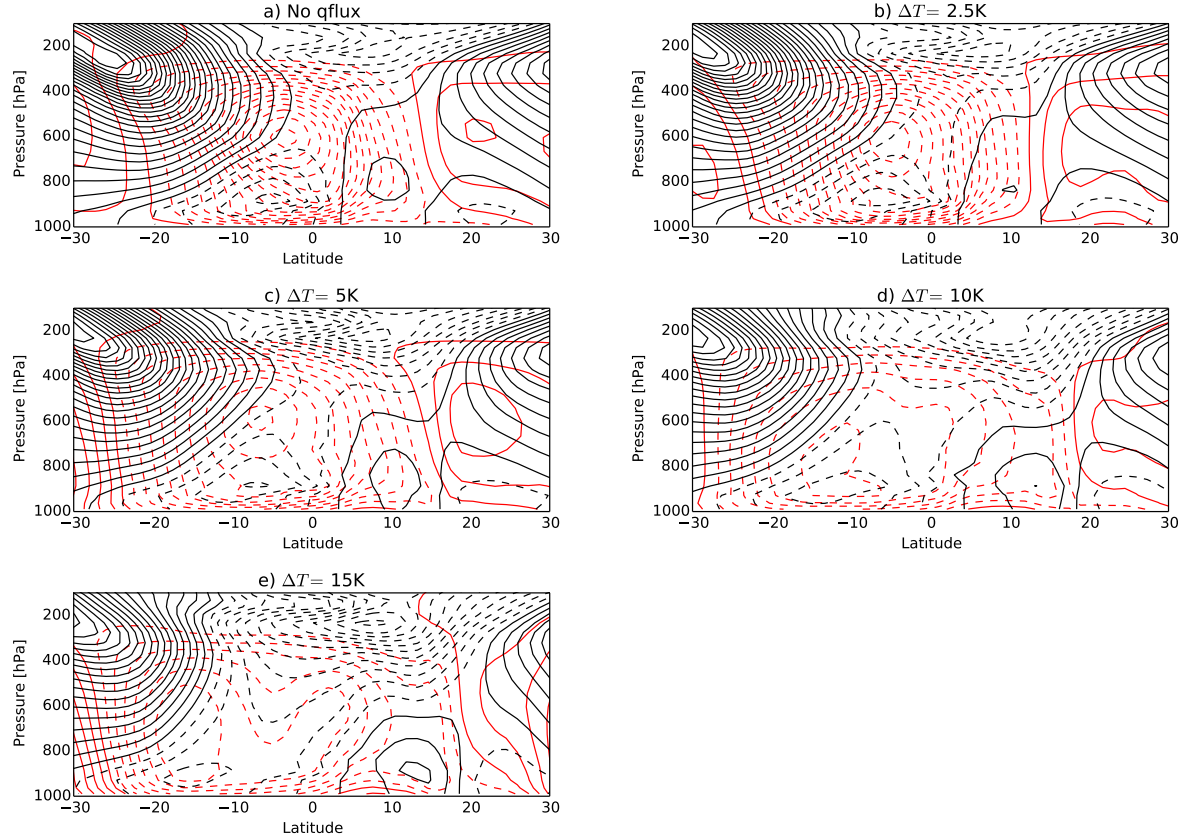
575 FIG. 3. a), b), c) Summer-time precipitation (blue contours) and winds at the lowest model level (arrows) for
 576 the experiment with no OHT (a), the experiment with interactive OHT and $\Delta T = 10K$ (b) and the experiment
 577 with the 1.5-layer parameterization. d), e), f) Moist static energy (MSE) at the lowest model level from the
 578 same experiments. Gray regions have MSE values outside the colorbar scale. g), h) OHT divergence from the
 579 experiments with interactive OHT.



580 FIG. 4. a), c) Hovmuller diagrams of the precipitation (a) and surface MSE (c), averaged over 100° to 235° E,
581 for the last four years of the land simulation with no OHT. b), d) Same for the land simulation with interactive
582 OHT and $\Delta T = 10K$. The horizontal black lines mark the southern edge of the continent. Note that the model is
583 initialized at year 0.



584 FIG. 5. a) Summer SSTs, averaged from 100° to 235° E, in the simulations with land and with ΔT varied
585 from 0K to 15K. The vertical line marks the southern boundary of the continent. b) Averaged summer surface
586 MSE in these simulations. c) Averaged summer precipitation in these simulations. d) Averaged summer specific
587 humidity in these simulations. e) Averaged summer OHT in these simulations.



588 FIG. 6. a) Summertime mean meridional circulation (MMC, red contours) and zonal winds (black contours)
 589 averaged over the land sector (100° to 235°E) in the land simulation with $\Delta T = 0\text{K}$. The contour intervals are 2
 590 $\times 10^9 \text{kg s}^{-1}$ for the MMC and 2ms^{-1} for the zonal wind. Dashed red contours denote counterclockwise circula-
 591 tion and dashed black contours denote negative zonal wind speeds. b) Same for the simulation with $\Delta T = 2.5\text{K}$.
 592 c) Same for the simulation with $\Delta T = 5\text{K}$. d) Same for the simulation with $\Delta T = 10\text{K}$. e) Same for the simulation
 593 with $\Delta T = 15\text{K}$.

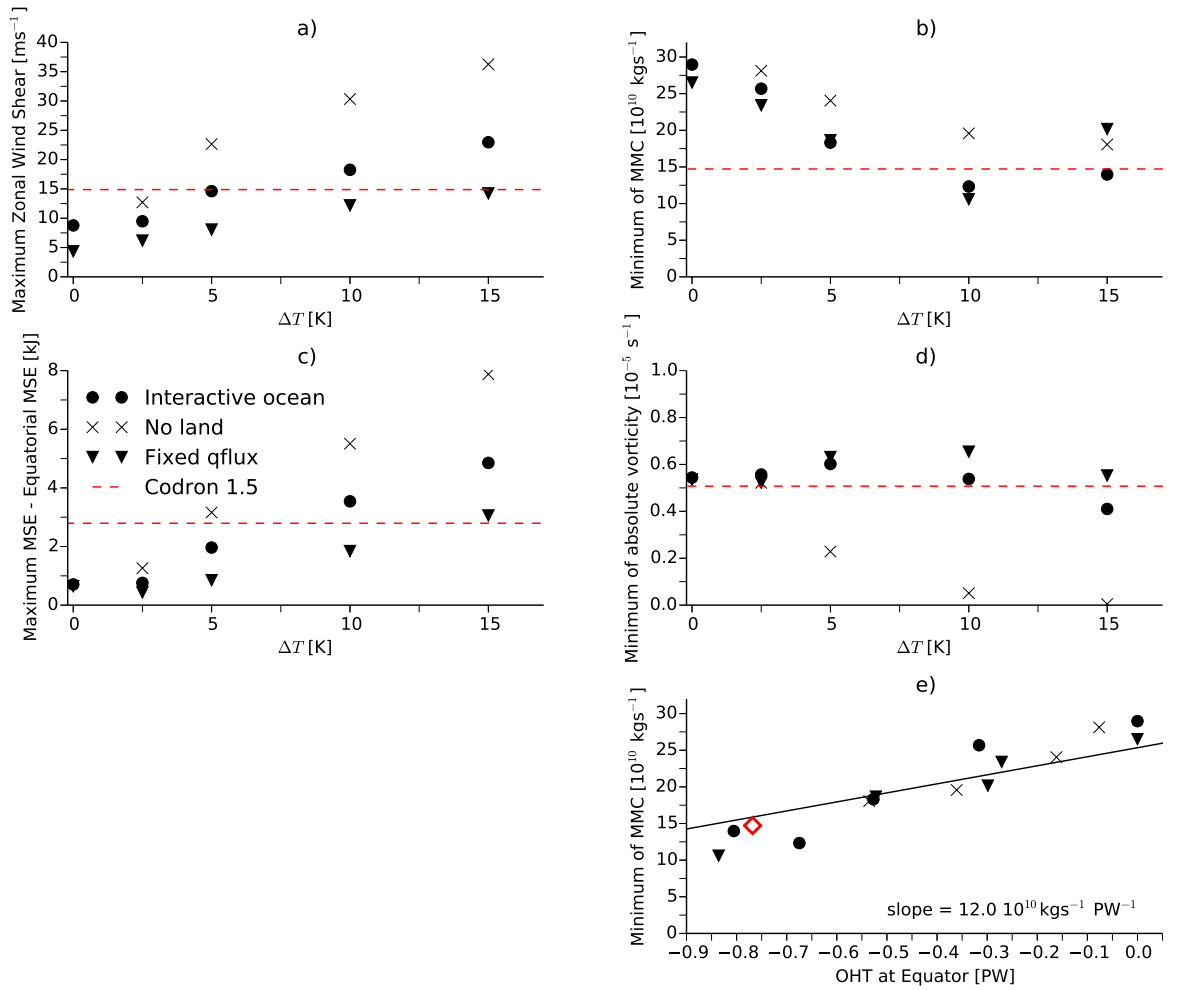


FIG. 7. a) Maximum of ($u(850\text{hPa}) - u(250\text{hPa})$), averaged over the land sector (100° to 235°E), between the equator and 20°N during the summer months for the simulations with land and interactive OHT (circles), the simulations with interactive OHT and no land (triangles) and with land and OHT fixed at it's annual-mean values (crosses). b) Minimum of the summertime mean meridional circulation (MMC) for the same simulations. c) Difference between maximum summer MSE and equatorial MSE at the equator for the same simulations. d) Minimum absolute vorticity polewards of 7°N during the summer of the same simulations. e) Minimum of the summertime MMC for the same simulations as a function of the equatorial OHT in the land sector. The line shows a linear least-squares fit. In panels a) to d) The dashed red lines shows the results from the experiment with the Codron (2012) 1.5-layer parameterization, and the red diamond in panel e) shows the minimum summertime MMC and equatorial OHT for the experiment with the Codron parameterization.

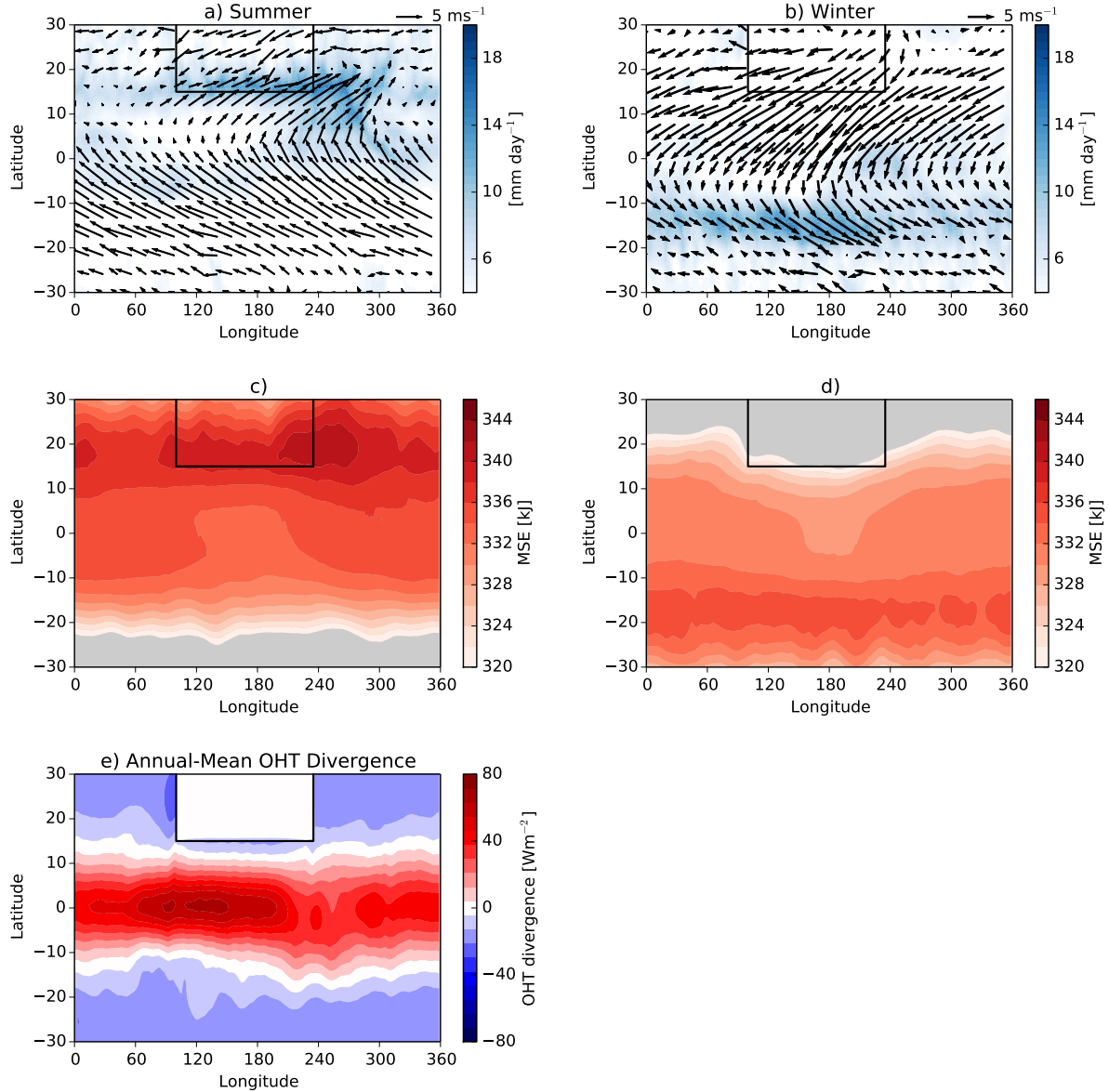


FIG. 8. a) Summer precipitation (contours) and near-surface winds (arrows) in the simulation with land and OHT fixed at its annual-mean value from the ΔT simulation with land. c) Summer near-surface MSE from the same simulation. b), d) Winter precipitation and near-surface MSE from the same simulation. e) Annual-mean OHT divergence in the $\Delta T = 10K$ simulation with land.

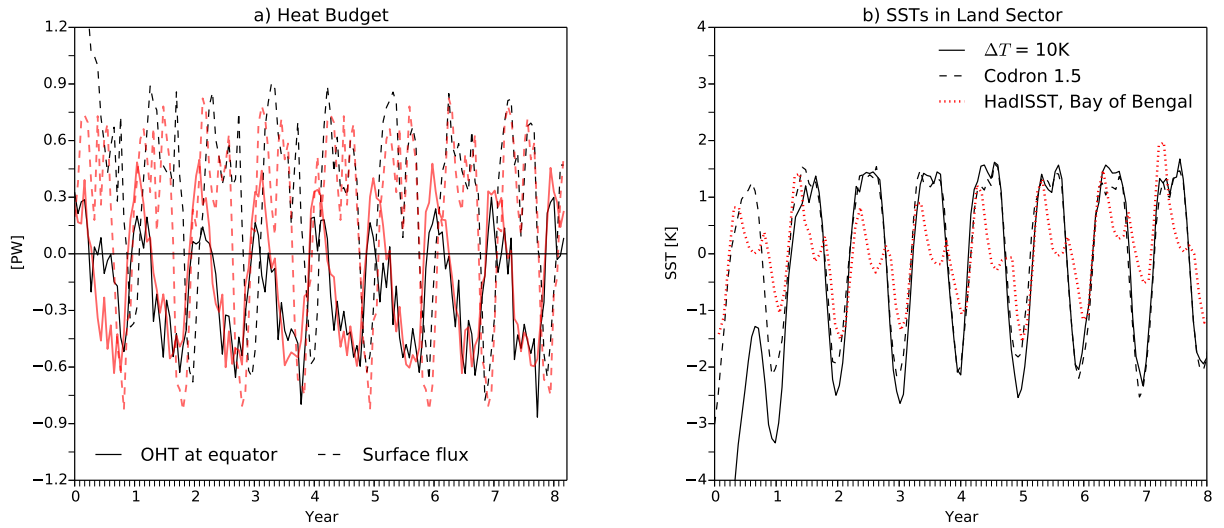
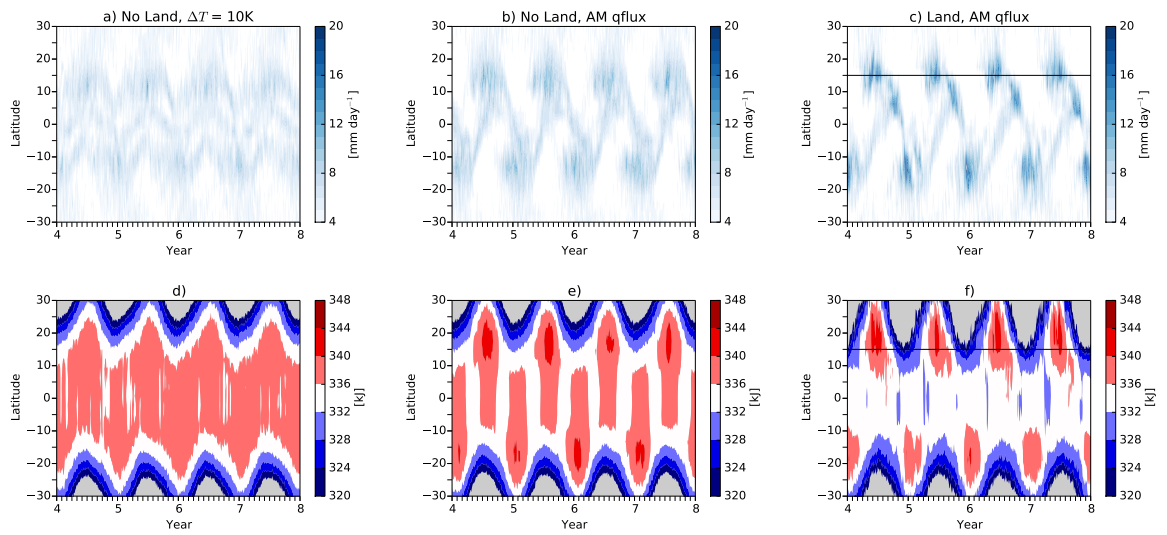


FIG. 9. a) Ocean heat transport across the equator, integrated from 100° to 235°E (solid lines) and net surface flux integrated over the region 100° to 235°E and 0 to 15°N (dashed lines), from the land simulation with $\Delta T = 10\text{K}$ (black lines) and with the 1.5-layer parameterization (red lines). The heat transport is positive when it is northward. b) SSTs averaged over the region (100° to 235°E and 0° to 15°N) from the simulation with $\Delta T = 10\text{K}$ (solid black line), the simulation with the 1.5-layer parameterization (dashed black line) and SSTs averaged over the Bay of Bengal (80° to 95°E and 0° to 15°N) for the period 2012 to 2016, taken from the HadISST dataset (dotted red line).



615 FIG. 10. a), d) Hovmöller diagrams of zonal-mean precipitation (a) and meridional gradient of surface MSE
 616 (d) for the last four years of the simulation with no land and $\Delta T = 10K$. b), e) Same for the simulation without
 617 land and with OHT fixed at its annual-mean value from the $\Delta T = 10K$ simulation. c), f) Same for the simulation
 618 with land and with OHT fixed at its annual-mean value from the $\Delta T = 10K$ simulation.